AIAA JOURNAL
Vol. 40, No. 8, August 2002

Closed-Loop Neurocontroller Tests on Piezoactuated Smart Rotor Blades in Hover

Michael G. Spencer,* Robert M. Sanner,† and Inderjit Chopra‡
University of Maryland, College Park, Maryland 20742

On-blade smart structure actuators are capable of actively altering the aerodynamic loads on rotor blades. With a suitable feedback control law, such actuators could potentially be used to counter the vibrations induced by periodic aerodynamic loading on the blades with lower weight penalties than the previous actuation methods and without the bandwidth constraints. We cover the development and testing of a new, robust individual blade control methodology for rotor vibration suppression using piezoactuated trailing-edge flaps and active twist tip rotors. The controller uses a neural network to learn to actuate the trailing-edge flap, thus adaptively suppressing the blade or hub vibrations. In this application, no offline training is performed. Instead, a neural network is used in real time to command adaptively the actuator deflections, thus reducing vibrations. Closed-loop experimental tests with piezoactuated-scale rotor systems were conducted on the University of Maryland hover test stand. The results include two different Mach-scale smart rotor systems (trailing-edge flaps and active tip twist) that were controlled by the same adaptive neurocontrol algorithm. These tests demonstrate the controller's robust ability to learn to control successfully the rotor vibrations with no a priori information about the blade/actuator structure or the aerodynamic loading.

I. Introduction

THE major source of helicopter vibration is the main rotor, which transmits oscillatory forces and moments through the hub to the airframe. The blade loads are generated by the unsteady aerodynamics at the rotor disk. For a rotor with N_b blades, the oscillatory $(N_b - 1)$/revolution, N_b/revolution, and $(N_b + 1)$/revolution blade loads are transmitted as exciting hub forces and moments to the vehicle at a dominant frequency of N_b/revolution (Ref. 1). Higher harmonic control (HHC) is an active vibration control approach that has been shown to be effective in suppressing helicopter vibrations. An HHC system excites the blade pitch at higher harmonics of the rotor rotational speed, generating new unsteady airloads that combine with oscillatory inertial loads to cancel the harmonics of the blade loads that cause hub vibrations. The helicopter vibrations are thereby suppressed at the source.[1–3]

One method that has been extensively investigated is active blade root pitch control using swashplate oscillations. The swashplate is activated in the collective, longitudinal cyclic and lateral cyclic modes at N_b/revolution resulting in blade pitch oscillations at the frequencies of $(N_b - 1)$/revolution, N_b/revolution, and $(N_b + 1)$/revolution in the rotating frame.[1] HHC methods have been applied successfully using numerical simulations,[1–4] wind-tunnel tests,[5–8] and full-scale flight tests,[9–11] producing reductions in vibration from 25 to 90%.

Although capable of reducing vibrations, these control systems require high actuation power and involve large weight penalties. Also, the swashplate actuation is limited to N_b/revolution. These drawbacks lead to research into individual blade control (IBC)[10–14] systems, where the pitch of each blade is controlled separately at any desired frequency. The feathering of the complete blade requires large actuation forces, and early IBC methods used hydraulic devices that incur large weight penalties. The introduction of smart structure materials into rotor blades has provided the potential for actuation devices that are lightweight and can operate over a wide bandwidth of frequencies.[13]

Recently, methods of actively controlling vibration have shifted to trailing-edge flaps. There are two basic types of flaps, servoflaps and plain flaps. The servoflaps extend beyond the nominal structure of the blade and, therefore, induce pitching moments for the control of the blade. The plain flap is part of the blade, just as the aileron of an aircraft wing, and induces lift as well as moments to control oscillatory blade motion. The advantage of the plain flap over the servoflap is that it has lower drag and normally requires less activation power. Various scaled rotor models with plain trailing-edge flaps have been designed and tested that demonstrate the capability of these systems to reduce the vibratory hub loads effectively. Feasibility studies have been carried out to show their potential for full-scale rotor systems to minimize actively vibratory loads.[15–20]

Our earlier efforts[21–23] explained the development of the neurocontrol algorithm that provides a new method capable of improved performance over the normally used controllers. Numerical simulation results were used to demonstrate the ability of the controller to learn to minimize blade and hub vibratory loads. This paper presents the results from real-time, closed-loop vibration control tests with the neurocontrol algorithm on scale rotor blades in hover. Two different sets of Mach-scale rotor blades with different smart structure actuators were tested to demonstrate the robust learning capability of the controller. The paper is organized as follows. A brief review of the neurocontrol algorithm is first presented. The controller implementation and the test configuration are explained, followed by a discussion of the hardware and test results.

II. Neural Network Control Algorithm

HHC provides a frequency-domain approach for controlling helicopter vibrations by representing the inputs and outputs in sine and cosine components that are normally restricted to a few selected frequencies. In contrast, the neurocontrol strategy is developed directly in the time domain. A radial basis network structure is used as the approximator for the command input because it provides a highly adaptive, splinelike solution for complex, nonlinear functions. The period T_{pd} is divided into N evenly spaced nodes, and associated with each node is a radial basis function $g(x, k)$. The

Received 30 January 2001; revision received 18 December 2001; accepted for publication 30 January 2002.

*Graduate Research Assistant, Alfred Gessow Rotorcraft Center, Department of Aerospace Engineering; currently Assistant Professor, Department of Aeronautics and Astronautics, Naval Postgraduate School. Member AIAA.

†Associate Professor, Alfred Gessow Rotorcraft Center, Department of Aerospace Engineering. Member AIAA.

‡Professor and Director, Alfred Gessow Rotorcraft Center, Department of Aerospace Engineering. Member AIAA.

control input is represented as the output of a single hidden layer network:

$$\delta(t) = \sum_{k=0}^{N-1} \gamma_k g[a\sigma(t) - k] \tag{1}$$

where g is the neural computational basis function, γ_k is the output weight for each neuron, a is the scaling parameter that determines the width of the neural function, $\sigma(t) = (t \bmod T_{\text{pd}})$ is the periodized time, and N is the total number of neural elements. A basis function that is computationally fast, efficient, and particularly convenient for real-time applications is the second-order B spline, shown in Fig. 1 in comparison to a typical Gaussian function. Note that the a and k are fixed in this formulation and that only the output weights γ_k are adjusted during operation.

One advantage of this type of network is the ease of characterizing the accuracy of the resulting approximation given the number of computing elements employed. For an r time continuously differentiable function ($r = 1$ for second-order B spline) the achievable uniform approximation accuracy provided by such an expansion, using the optimal coefficients $\gamma_{i,k}$, scales an $\mathcal{O}(a^{-1})$ (Ref. 24). The variable a is a scaling parameter that controls the accuracy of the approximation, and the total number of computing elements N is chosen so that the resulting collection $g(at - k)$ completely covers the domain on which the approximation is required.

Neural network approximation theory guarantees the accuracy specified earlier only for approximations on a bounded domain.[25,26] However, because the optimal input is known to be periodic with known period T_{pd}, then the approximation is in fact required only on the bounded time interval $[0, T_{\text{pd}}]$. Estimates for other values of time can then be reflected into this interval by periodicity using $\sigma(t)$.

The neural network approximation at any point in time $t \in [0, T_{\text{pd}}]$ is, therefore, a weighted sum of the influence of each of the evenly spaced neural elements. The neural approximation, using a second-order B spline for g, as shown in Fig. 2, is effectively the piecewise linear estimate to the unknown function $f(t)$. The accuracy of the estimate depends on the number of elements and the correct knowledge of the output weights. The correct set of weights is determined by the learning process, which itself depends on the control problem and will be developed in the following sections.

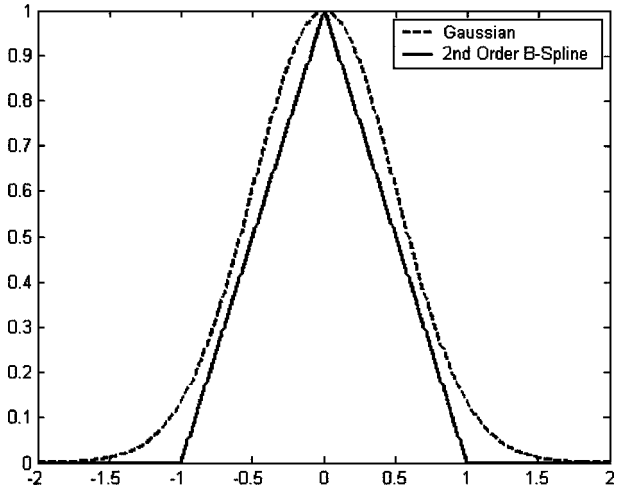

Fig. 1 Gaussian and second-order B spline as radial basis functions.

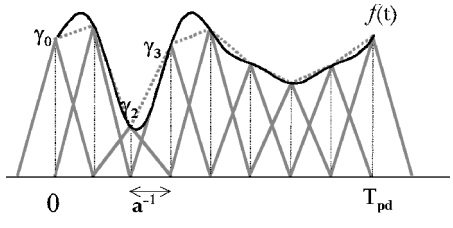

Fig. 2 Unknown periodic function $f(t)$ divided into N segments with second-order B-spline functions as the neural computational elements; network weights γ_k are associated with the approximation to the function $f(t)$.

The neural network controller is developed in a discrete time frame by sampling the loads and control inputs on a per rev basis. The network is developed to approximate the control input necessary to minimize the vibratory component of the loads in the measured signal $\boldsymbol{y}$. The steady-state output obtained from this input can be expressed as

$$\boldsymbol{y} = \boldsymbol{y}_0 + \boldsymbol{H}\gamma + \nu \tag{2}$$

where $\boldsymbol{y}$ consists of evenly spaced samples of the blade or hub loads on the interval $\tau = [0, T_{\text{pd}}]$. The vector γ contains the coefficients γ_k from Eq. (1), and ν is measurement noise. Vector $\boldsymbol{y}_0$ contains samples of the uncontrolled load variations (when $\gamma = 0$). The columns of $\boldsymbol{H}$, denoted as $\boldsymbol{h}_k$, represent the components of the response due to each neural basis function g_k, that is, the $(k+1)$th column of $\boldsymbol{H}$ is the response $\boldsymbol{y}$ obtained if $\boldsymbol{y}_0 = 0$ and $\delta(t) = g_k[\tau(t)]$.

The optimal set of control inputs is determined by minimizing the cost function J_{NN}

$$J_{\text{NN}} = \boldsymbol{y}^T \boldsymbol{W}_y \boldsymbol{y} + \gamma^T \boldsymbol{W}_\gamma \gamma \tag{3}$$

where $\boldsymbol{W}_y$ and $\boldsymbol{W}_\gamma$ are weighting functions for the vibratory loads and the control inputs, respectively. The optimal network weights γ are determined by setting $\partial J_{\text{NN}}/\partial \gamma = 0$ and solving for γ_{opt} as

$$\gamma_{\text{opt}} = -\left(\boldsymbol{H}^T \boldsymbol{W}_y \boldsymbol{H} + \boldsymbol{W}_\gamma\right)^{-1} \boldsymbol{H}^T \boldsymbol{W}_y \boldsymbol{y}_0 \tag{4}$$

Effective vibration suppression depends on knowledge of $\boldsymbol{y}_0$ and $\boldsymbol{H}$, which may be difficult to determine a priori. An adaptive algorithm was developed using a Kalman filter to estimate the uncertain information online. The Kalman filter states are the estimates of the neural response vectors $\boldsymbol{h}_k$ and the uncontrolled response $\boldsymbol{y}_0$. The network coefficients γ are then dynamically updated to minimize J_{NN} given the current estimates of the state parameters, for example,

$$\hat{\gamma}_n = \arg\min_{\gamma} \left\{ W_y \|\hat{\boldsymbol{H}}_n \gamma + \hat{\boldsymbol{y}}_{0,n}\|^2 + \gamma^T \boldsymbol{W}_\gamma \gamma \right\} \tag{5}$$

where $\hat{\boldsymbol{H}}_n$ and $\hat{\boldsymbol{y}}_{0,n}$ are the Kalman filter estimates of $\boldsymbol{H}$ and $\boldsymbol{y}_0$ at iteration n, respectively. Our previous results with the control algorithm demonstrated the control of vibratory hub loads by using comprehensive rotor analysis UMARC to provide a pseudo-time-marching simulation of the forward flight conditions.[22,23] The next step in the controller development is to validate the algorithm with real-time, closed-loop control tests utilizing active rotor systems.

III. Real-Time Closed-Loop Tests

A. Test Objectives

Two types of Mach-scaled smart rotor models (6-ft diam) with piezoactuated trailing flaps and piezo plus bending–torsion coupling actuated blade tips, respectively, were tested successfully in hover and demonstrated their effectiveness in open-loop tests. The tests were conducted at Mach-scale speeds (up to 2000 rpm), and they successfully demonstrated the control authority and hardware durability.[19,27]

First, the initial hardware-in-the-loop tests of the neurocontroller were developed for a two-bladed rotor with a single rotor blade with an active flap operating in hover. The adaptive learning capability of the controller was demonstrated by allowing the controller to minimize blade root flapping moment vibrations with no a priori information of the blade or the flight conditions. This system was subject to periodic vibratory loads due to the out-of-track rotor (dissimilar blades) and loads induced by the actuator. Two types of tests were conducted. The first tests were to demonstrate the neurocontroller learning to counter the background vibrations arising from the nontracked rotor. The second tests were to demonstrate the neurocontroller inducing vibratory loads at specific frequencies as would be necessary for vibration reduction of the rotor in forward flight situations.

Second, to further demonstrate the versatility of the neurocontroller, these hover tests were repeated using the same control

algorithm but with a different smart rotor. This rotor used an active tip to alter the aerodynamics to reduce vibrations.

B. Controller Hardware

To implement the neurocontrol algorithm, a dedicated Pentium III 550-MHz personal computer with a National Instruments PCI-MIO-16E-1, 12-bit data acquisition (DAQ) board was used to host the controller and perform the data acquisition and waveform generation. This controller hardware setup provided an efficient and cost-effective system to implement the real-time control algorithm directly in Visual C++. The DAQ board hardware commands such as read and write of data from the input and output channels were implemented through the libraries of C code commands provided with the hardware.[28–30] The neurocontroller output solution had output limits of ±5 V from the DAQ board. The output signal was amplified with Trek 50/750 amplifiers to ±180 V and transmitted through a separate set of slip ring channels to the piezoactuator. The flapping moment strain-gauge signal was transmitted through a different separated set of slip ring channels to the signal conditioners in the control room.

The control algorithm requires the quasi-steady-vibratory signal sampled at N evenly sampled points within a single revolution, and similarly, the resultant command output is computed for N evenly spaced points within a single revolution. To ensure the input vector and resultant output control signal vectors were synchronized, the intertriggered, continuous, double-buffered capabilities of the DAQ board were used. The double-buffer feature enables the controller to update and control the output sequence simultaneously. The length of the buffer and sampling rate were determined as part of the hardware initialization such that a half buffer covered one rotor revolution. The numerical C++ package used to perform the matrix/vector computations within the Kalman filter and optimizations steps was the Template Numerical Toolkit (TNT).[31] The following test results reflect the implementation of the described control system.

C. End-to-End Controller Testing

Before the new control algorithm and computer were used on an actual rotor system, a set of end-to-end shakedown tests were developed and performed on the hardware and software. These tests were designed to achieve three goals. The first was to ensure that the hardware interface elements of the code were functioning properly. The second goal was to ensure that the control algorithm would generate the correct output solution for a known, given input to the A/D hardware. The final goal was to use the tests to determine the appropriate values of the free parameters within the algorithm for the closed-loop tests with the actual rotor system.

For the shakedown tests, a function generator was used to provide known input signals of various shapes at different frequencies and amplitudes. When the signal to minimize in the cost function was the sum of the input and the neural network solution, the controller would learn to cancel the input by learning its negation. The measured inputs and control outputs were compared and used to verify that the controller was indeed learning the desired results. The following sections explain the various aspects and results of the end-to-end tests.

1. Initialization

The success of this controller depends in part on the inherent compensation of noise with the covariance models ($\boldsymbol{R}_n$ and $\boldsymbol{Q}_n$) within the Kalman filter. The nonrotating background signal was measured at ±0.01 mV, indicating very low sensor noise. The strain-gauge signals for the spinning rotor were low-voltage measurements, less than 100 mV, and were on the order of the normalized load values encountered in the simulations. The test input signal was to be up to ±5 V with various levels of noise added. The noise was assumed uncorrelated; therefore, the initial noise covariance estimate was set at $\boldsymbol{R} = 1.0\boldsymbol{I}$, where $\boldsymbol{I}$ is the identity matrix. The Kalman filter state initial covariance was set to $\boldsymbol{P} = 3.0\boldsymbol{I}$. The plant covariance was set to $\boldsymbol{Q} = 0.01\boldsymbol{I}$. These values were sufficient for the initialization tests and were kept constant for the subsequent tests. The initial values of the Kalman filter states, $\boldsymbol{h}_k$ and $\boldsymbol{y}_0$, were set to zero, effectively giving the controller no a priori information about the blade, actuator or the aerodynamics. Likewise, the initial network weight vector γ was set at small random numbers (order 1×10^{-3}).

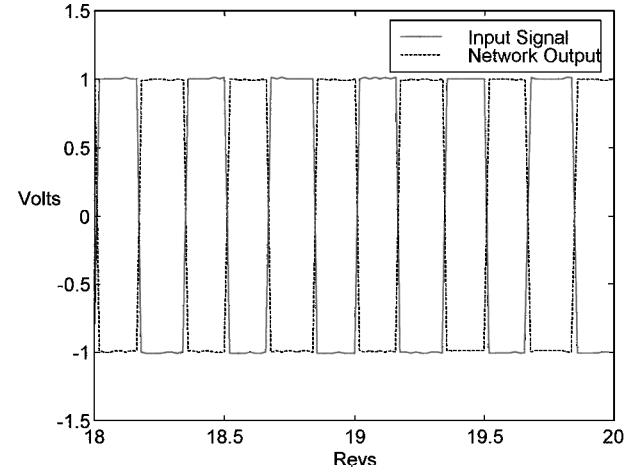

Fig. 3 Controller initialization tracking test results, W_γ 0.01 and 0.5; controller learns negative of test load signal. Used ± 1 V square wave as test signal.

2. Cost Function Terms

In addition to the Kalman filter covariances, the other free parameters within this control application are the weights associated with the neural network cost function. One set of variables are the relative weights associated with each load: W_x, W_y, W_z, W_{mx}, W_{my}, and W_{mz}. Because the shakedown tests and subsequent experiments involved a single vibratory load, the relative load weights were set to zero, except W_z, which was set to $W_z = 1$.

The other elements in the cost function are the weights associated with the control output $\boldsymbol{W}_\gamma$, which have a direct effect on the performance of the controller. The control output weight matrix contains relative weights that apply to the magnitude and the rate of change of the output solution. The weight matrix is given by

$$\boldsymbol{W}_\gamma = (\alpha\boldsymbol{I} + \beta\boldsymbol{D}^T\boldsymbol{D})\kappa \tag{6}$$

where α is the magnitude weight and β is the rate of change weight. The matrix $\boldsymbol{D}$ provides a circulant finite difference approximation for the rate of change of the command outputs. The overall gain κ provides the relative scaling between the squared load terms and the squared output terms so that neither set of terms numerically dominates the cost function.

The end-to-end tests with the function generator were used to find the values of α, β, and κ such that the control output solution would cancel the known input signal. A square wave of magnitude ±1 V was used as the load signal from the function generator. The overall gain was determined such that the order of the control output terms of the cost function were of the same order as the load terms. The gain was determined as $\kappa = \frac{1}{2000}$. The values for α and β were adjusted until the input signal was negated as shown in Fig. 3. The resultant control output was opposite of the input and was achieved with $\alpha = 0.01$ and $\beta = 0.5$.

3. Caution Terms

To prevent large-amplitude learning transients from the neurocontroller, cautionary limits of 0.1 V were applied as the maximum allowable amount of increase of the outputs from the previous revolution. In addition to the revolution-by-revolution limits, an overall maximum limit (±1.4 V) was applied to the output to prevent large voltages to the piezoactuators that would cause depoling or failure. This limit was set to correspond to a maximum piezoactuation of 180 Vrms.

IV. Results and Discussion

A. Trailing-Edge Flap Rotor

The rotor system in the first set of tests was a two-bladed piezoactuated rotor developed for the Mach-scale active rotor tests.[27] Both blades had trailing-edge flaps; however, only one blade was actively controlled by the neurocontroller. Whereas the blades had been tested at near Mach-scale speeds, the initial neurocontrol tests

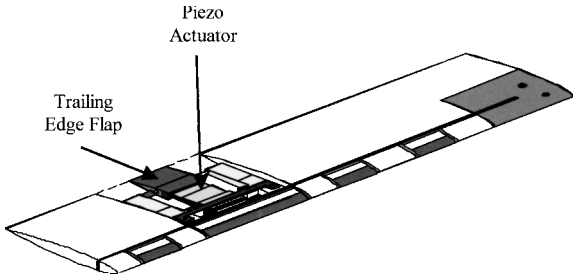

Fig. 4 Schematic of Mach-scale blade with piezoactuated trailing-edge flap.

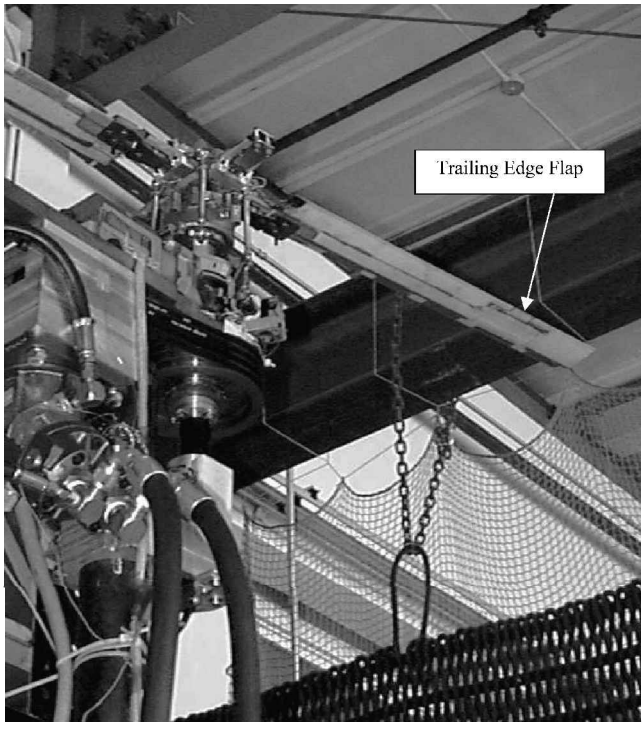

Fig. 5 Scale rotor blade with trailing-edge flap; two-bladed rotor on hover tower.

were conducted at slower speeds (<600 rpm) as a measure of caution to not damage the blades or the rotor. The blade radius was 36 in., and the trailing-edge flap span was 1.5 in. The rotor blades were mounted on a strain-gauge instrumented bearingless hub. Instead of controlling a fixed frame hub load, the rotating frame flexbeam flapping moment signal was the vibratory load source used by the neurocontroller. The schematic of the scale rotor blade with the piezoactuated trailing-edge flap is shown in Fig. 4. The actual active blade is shown on the rotor tower in Fig. 5.

1. Background Test Results

The cyclic settings for the rotor were 0.03 deg lateral and 0.3 deg longitudinal with collective effectively zero. This setting resulted in a minor 1P (1/rev) blade flapping moment for the hover test conditions with the rotor operating at 500 rpm (8.3 Hz). The first closed-loop test with the neurocontroller was to allow it to minimize the background vibration. Figure 6 shows the time history of the flapping moment response with the neurocontroller active. The controller begins updating immediately and by rev 15 has achieved the maximum vibration reduction possible. Figure 7 shows the comparisons of the flapping moment response, and clearly the dominant 1P vibration has been reduced. Indeed, the neurocontroller has reduced the total vibrational energy from 0.3038 to 0.0697, a 73% reduction. Moreover, the controller has achieved a broadband reduction in vibration, exhibited by significant reductions up to 5P.

The frequency spectrum of the trailing-edge flap input command over the last revolution is shown in Fig. 8. The actual flap deflection

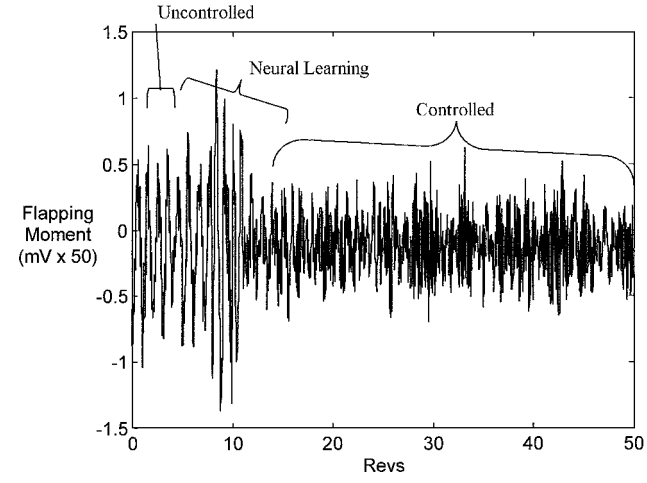

Fig. 6 Time history plot of background vibration suppression; blade root flapping moment at rotor speed of 500 rpm (8.3 Hz).

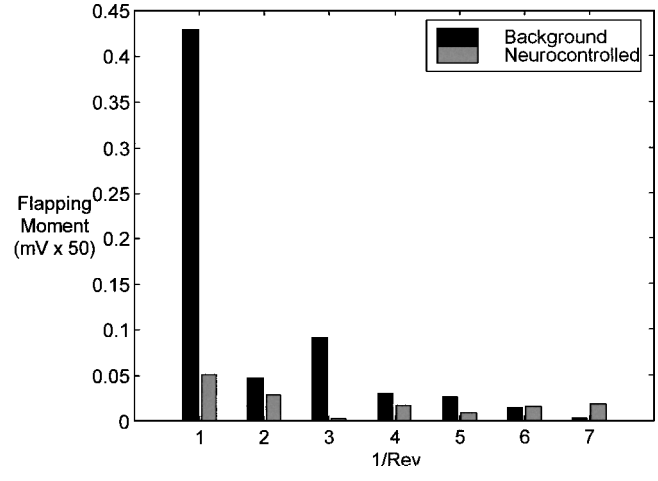

Fig. 7 Flapping moment harmonic spectrum comparison; blade root vibratory loads for rotor at 500 rpm (8.3 Hz).

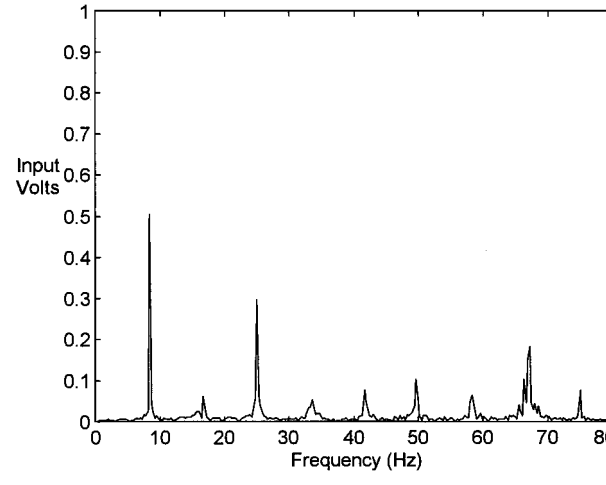

Fig. 8 Frequency spectrum for neural network control input for background suppression test; blade root vibratory control for rotor at 500 rpm (8.3 Hz).

angle was measured from a Hall effect sensor located on the blade. The flap motion data were acquired with a separate data acquisition computer that was not synchronized with the control computer; therefore, the two plots (Figs. 8 and 9) do not represent the exact same moments in time. The flap motion data were collected after the controller had achieved a converged solution. Figure 9 shows a time history for one rev of the measured trailing-edge flap motion after the converged neurocontroller solution had been achieved.

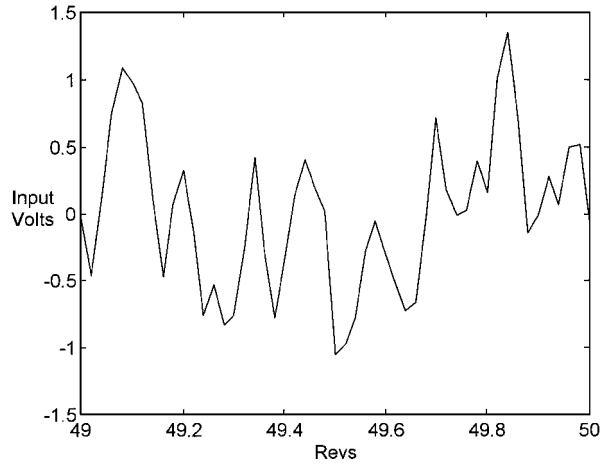

Fig. 9 Final revolution of neural network output: background suppression; blade root flapping moment control of rotor at 500 rpm (8.3 Hz).

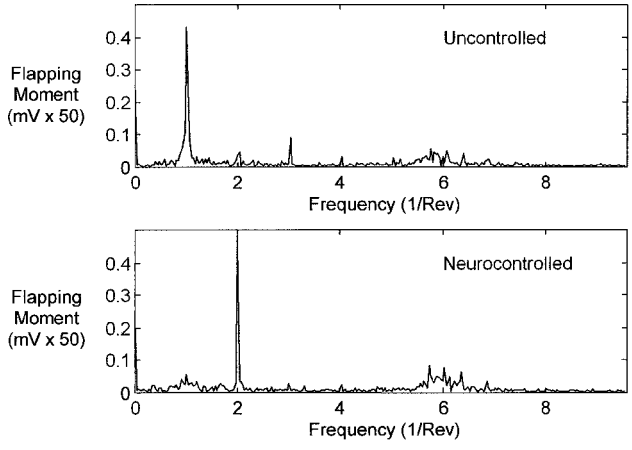

Fig. 10 Flapping moment spectrum comparison between uncontrolled and neurocontrolled induced-load test; desired induced load of 0.1 mV at 2P, rotor speed at 500 rpm (8.3 Hz).

2. Induced-Load Tests

The next tests were designed to demonstrate the controllers' ability to learn not only to control the background vibrations but also to induce other loads at specific frequencies. This task demonstrates the ability of the controller to track a user-specified load profile that simulates the controller learning to control more complex vibratory loads such as appear in forward flight. The first such test involved the controller inducing a specified vibratory flapping moment strain-gauge signal of 0.1 mV at a frequency of 2P. The comparison between the controlled and uncontrolled frequency spectrum for this test is shown in Fig. 10. The neurocontroller canceled the 1P and 3P background vibrations while simultaneously inducing the desired 2P load.

The described background suppression and 2P induced-load tests successfully demonstrated the controller's ability to minimize and/or induce vibrations while accounting for the system dynamics. In each case, the controller begins the learning process with no a priori information about the blade, the actuator, or the dynamics. The controller adaptively learns in real time while simultaneously controlling the system.

B. Active Twist Tip Rotor

The final tests were designed to demonstrate that the new controller could actually operate independently of the specific actuator. The neural network learns the actuator dynamics, as well as the blade response and actuator inputs[22]; therefore, the performance should be similar if tested with a new and different actuation system. The rotor system used in the tests was a new set of rotor blades that had the outer 10% of the blade free to rotate independent of the main blade. The tips were driven by a piezoactuated, bending–torsion composite coupled beam embedded within the rotor blade.[32] A four-bladed rotor was used; however, as with the previous tests, only one blade was controlled. A schematic of the new piezoactuated tip twist rotor blade is shown in Fig. 11, and the actual rotor is shown on the hover test stand in Fig. 12. These blades have the same length and chord as the trailing-edge flap blades; however, the mass and stiffness properties are different due to the complex, embedded actuator system.

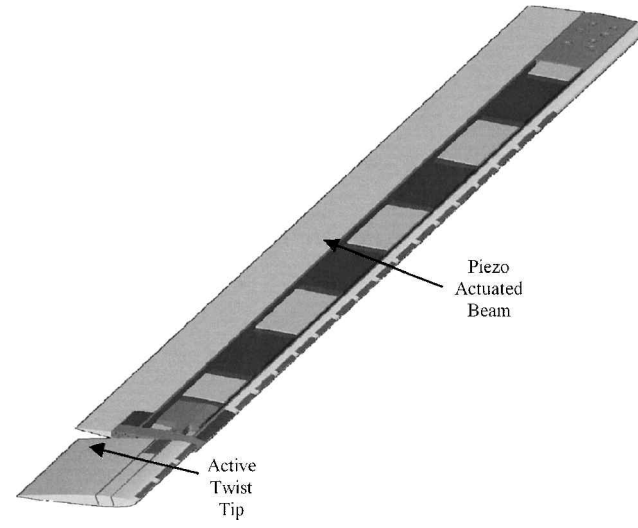

Fig. 11 Schematic of active tip twist rotor blade.

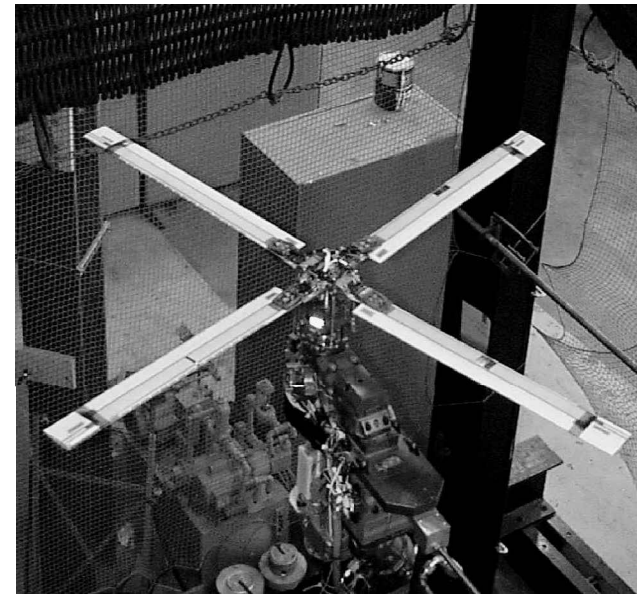

Fig. 12 Active tip twist rotor on hover stand.

The same types of tests were performed with this rotor as with the earlier trailing-edge flap rotor. The blade root flapping moment signal was used as the control parameter, and the outputs to the blade were the voltages to the power amplifiers. The same control algorithm was used, and the only modification was to change the maximum output voltage to 2.83 V. The same initializations were used as in the earlier tests.

The following active tip rotor test results were for the hover tests conducted at a rotor speed of 2000 rpm (33.3 Hz). The rotor cyclic inputs were as close to zero as possible; however, a 1P background vibration remained. The background suppression test was conducted with the controller learning to minimize the dominant 1P vibration. The harmonic vibration comparison is shown in Fig. 13, demonstrating that the controller has achieved a 98% reduction.

The induced-load tests were also conducted at different rotor harmonics. A multifrequency load was also tested for this new rotor,

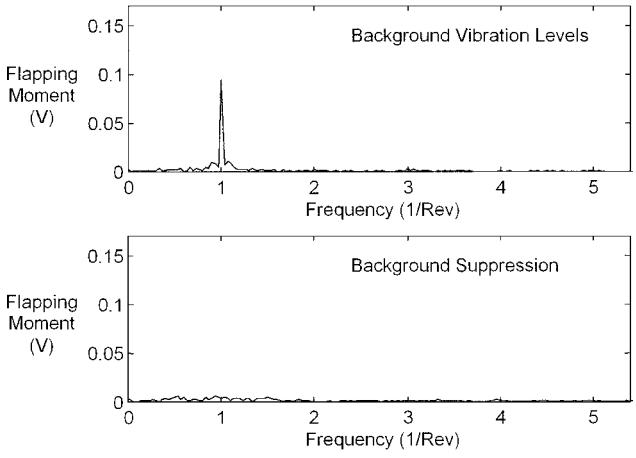

Fig. 13 Flapping moment frequency spectrum comparison for active tip twist rotor blade; blade root vibratory load for rotor at 2000 rpm (33.3 Hz).

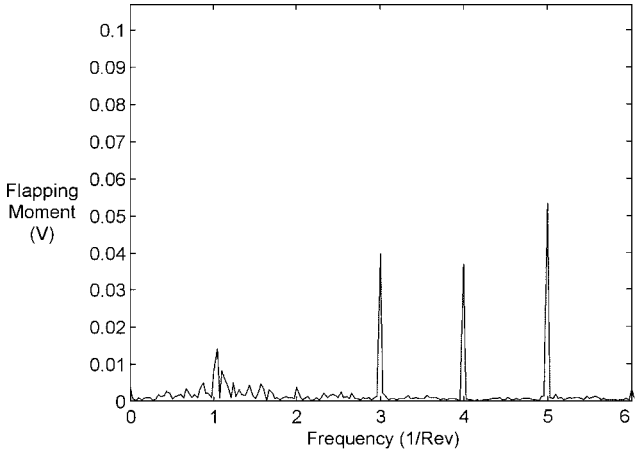

Fig. 14 Flapping moment results for combined induced-load test: active tip twist rotor blade with desired loads 45 mV at 3P, 40 mV at 4P, and 55 mV at 5P; rotor at 2000 rpm (33.3 Hz).

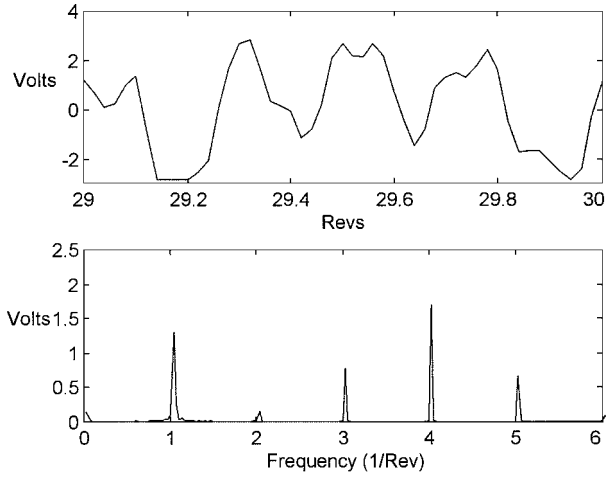

Fig. 15 Neurocontrol inputs for combined induced-load test: active tip twist rotating blade, desired loads 45 mV at 3P, 40 mV at 4P, and 55 mV at 5P; rotor at 2000 rpm (33.3 Hz).

illustrating the types of loads the controller would be required to use in forward flight conditions. The controller was tasked to induce simultaneously loads of 45 mV at 3P, 40 mV at 4P, and 55 mV at 5P. Figure 14 shows spectrum of the resultant load, indicating that the controller has achieved the multiload task. The command input solution and its spectrum are shown in Fig. 15, demonstrating again that the controller learns a broad spectrum input to achieve the control task.

V. Conclusions

These closed-loop tests with two different Mach-scale smart rotor systems demonstrate the neurocontroller's robust ability to learn successfully to control the rotor vibrations with no a priori information about the blade, the actuator, or the aerodynamic loading. The controller uses a neural network to learn to drive the smart rotor actuator, thus adaptively suppressing the blade vibrations. These tests demonstrated that no offline training was necessary. Instead, the neural network simultaneously learned in real time while adaptively commanding the actuator to reduce vibrations.

Acknowledgments

This work is supported by the U.S. Army Research Office under Grant MURI: DAAH-04-96-10344 with Gary Anderson as Technical Monitor and by The Boeing Co. under Contract 575329 with Friedrich Straub as Technical Monitor.

References

[1]Nguyen, K., and Chopra, I., "Application of Higher Harmonic Control to Rotors Operating at High Speed and Thrust," *Journal of the American Helicopter Society*, Vol. 35, No. 3, 1990, pp. 78–89.

[2]Chopra, I., and McCloud, J. C., III, "A Numerical Simulation Study of Open-Loop and Adaptive Multicyclic Control Systems," *Journal of the American Helicopter Society*, Vol. 28, No. 1, 1983, pp. 63–77.

[3]Johnson, W., "Self-Tuning Regulators for Multicyclic Control of Helicopter Vibration," NASA TP 1996, March 1982.

[4]Davis, M. W., "Refinement and Evaluation of Helicopter Real-Time Self-Adaptive Active Vibration Controller Algorithms," NASA CR 3821, Aug. 1984.

[5]Molusis, J. A., Hammond, C. E., and Cline, J. H., "A Unified Approach to the Optimal Design of Adaptive and Gain Scheduled Controllers to Achieve Minimum Helicopter Rotor Vibration," *Journal of the American Helicopter Society*, Vol. 28, No. 2, 1983, pp. 9–18.

[6]Hammond, C. E., "Wind Tunnel Results Showing Rotor Vibratory Loads Reduction Using Higher Harmonic Blade Pitch," *Journal of the American Helicopter Society*, Vol. 28, No. 1, 1983, pp. 10–15.

[7]Shaw, J., and Albion, N., "Active Control of the Helicopter Rotor for Vibration Reduction," *Journal of the American Helicopter Society*, Vol. 26, No. 3, 1981, pp. 32–39.

[8]Shaw, J., Albion, N., Hanker, E. J., and Teal, R. S., "Higher Harmonic Control: Wind Tunnel Demonstration of Fully Effective Vibratory Hub Forces Suppression," *Journal of the American Helicopter Society*, Vol. 34, No. 1, 1989, pp. 14–25.

[9]Wood, E. R., Powers, R. W., Cline, C. H., and Hammond, C. E., "On Developing and Flight Testing a Higher Harmonic Control System," *Journal of the American Helicopter Society*, Vol. 30, No. 1, 1985, pp. 3–20.

[10]Walsh, D. M., "Flight Tests of an Open Loop Higher Harmonic Control System on an S-76A Helicopter," *Proceedings of the American Helicopter Society 42nd Annual Forum*, American Helicopter Society, Alexandria, VA, 1986, pp. 831–844.

[11]Polychroniodis, M., and Achache, M., "Higher Harmonic Control: Flight Tests of an Experimental System on SA 349 Research Gazelle," *Proceedings of the American Helicopter Society 42nd Annual Forum*, American Helicopter Society, Alexandria, VA, 1986, pp. 811–820.

[12]Ham, N. D., "Helicopter Individual-Blade Control Research at MIT 1977-1985," *Vertica*, Vol. 11, No. 1, 1987, pp. 109–122.

[13]Jaklin, S. A., Nguyen, K., Blaas, A., and Richter, P., "Full-Scale Wind Tunnel Test of a Helicopter Individual Blade Control System," *Proceedings of the American Helicopter Society 50th Annual Forum*, American Helicopter Society, Alexandria, VA, 1994, pp. 579–596.

[14]McKillip, R. M., Jr., "Periodic Control of the Individual Blade Control Helicopter Rotor," *Vertica*, Vol. 9, No. 2, 1985, pp. 199–225.

[15]Chopra, I., "Status of Application of Smart Structures Technology to Rotorcraft Systems," *Proceedings of the Royal Aeronautical Society's Innovations in Rotorcraft Technology*, London, 1997.

[16]Lee, T., and Chopra, I., "Design and Spin Testing of an Active Trailing Edge Flap Actuated with Piezostacks," *Proceedings of the 40th AIAA/ASME/ASCE/AHS/ASC Structures, Structural Dynamics, and Materials Conference*, AIAA, Reston, VA, 1999, pp. 2403–2413.

[17]Fulton, M. V., and Ormiston, R. A., "Small-Scale Rotor Experiments with On-Blade Elevons to Reduce Blade Vibratory Loads in Forward Flight," *Proceedings of the American Helicopter Society 54th Annual Forum*, American Helicopter Society, Alexandria, VA, 1998, pp. 433–451.

[18]Koratkar, N. A., and Chopra, I., "Analysis and Testing of a Froude Scaled Helicopter Rotor with Piezoelectric Bender Actuated Trailing Edge Flaps," *Journal of Intelligent Material Systems and Structures*, Vol. 8, No. 7, 1997, pp. 555–570.

[19]Koratkar, N. A., and Chopra, I., "Analysis and Testing of a Mach-Scaled Rotor with Trailing Edge Flaps," *AIAA Journal*, Vol. 38, No. 7, 2000, pp. 1113–1124.

[20]Dawson, S. et al., "Wind Tunnel Test of an Active Flap Rotor: BVI Noise and Vibration Reduction," *Proceedings of the 51st Annual Forum of the American Helicopter Society*, American Helicopter Society, Alexandria, VA, 1995, pp. 631–648.

[21]Spencer, M. G., Sanner, R. M., and Chopra, I., "Development of Neural Network Controller for Smart Structure Activated Rotor Blades," *Proceedings of the 39th AIAA/ASME/ASCE/AHS/ASC Structures, Structural Dynamics, and Materials Conference and AIAA/ASME/AHS Adaptive Structures Forum*, AIAA, Reston, VA, 1998, pp. 3326–3336.

[22]Spencer, M. G., Sanner, R. M., and Chopra, I., "Adaptive Neurocontrol of Simulated Rotor Vibrations Using Trailing-Edge Flaps," *Journal of Intelligent Material Systems and Structures*, Vol. 10, No. 11, 1999, pp. 855–871.

[23]Spencer, M. G., Sanner, R. M., and Chopra, I., "Neurocontrol of Simulated Full-Scale Rotor Vibrations Using Trailing Edge Flaps," *Proceedings of the 40th AIAA/ASME/ASCE/AHS/ASC Structures, Structural Dynamics, and Materials Conference and AIAA/ASME/AHS Adaptive Structures Forum*, AIAA, Reston, VA, 1999, pp. 2744–2752.

[24]Powell, M. J. D., "Theory of Radial Basis Function Approximation," *Advances in Numerical Analysis*, edited by W. A. Light, Vol. 2, Oxford Univ. Press, Oxford, 1992.

[25]Haykin, S., *Neural Networks, A Comprehensive Foundation*, Macmillan College Publ., New York, 1994.

[26]Sanner, R. M., and Slotine, J.-J. E., "Stable Adaptive Control of Robot Manipulators Using 'Neural' Networks," *Neural Computation*, Vol. 7, No. 4, 1995, pp. 753–790.

[27]Koratkar, N. A., and Chopra, I., "Analysis and Testing of Mach Scaled Rotor Model with Piezoelectric Bender Actuated Trailing-Edge Flaps for Helicopter Vibration Control," *Proceedings of the 40th AIAA/ASME/ASCE/AHS/ASC Structures, Structural Dynamics, and Materials Conference and AIAA/ASME/AHS Adaptive Structures Forum*, AIAA, Reston, VA, 1999, pp. 2380–2402.

[28]"PCI E Series User Manual," July ed., National Instruments, Pt. 320945C-01, Austin, TX, 1997.

[29]"NI-DAQ User Manual for PC Compatibles," Ver. 6.5, National Instruments, Oct. ed., Pt. 321644D-01, Austin, TX, 1998.

[30]"NI-DAQ Function Reference Manual for PC Compatibles," Ver. 6.5, National Instruments, Pt. 321645D-01, Austin, TX, Oct. 1998.

[31]Pozo, R., "Template Numerical Toolkit for Linear Algebra, Mathematical and Computational Sciences Division," National Inst. of Standards and Technology, URL: http://math.inst.gov [July 1999].

[32]Bernhard, A., "Smart Rotor with Active Blade Tips (SABT)," Ph.D. Dissertation, Dept. of Aerospace Engineering, Univ. of Maryland, College Park, MD, Feb. 2000.

A. Chattopadhyay
Associate Editor